High Temperature Materials and Processes, Vol. 7, No. 1, 1986, 63-81

Strain Rate and Temperature Dependence of Deformation and Fracture Behaviour of a Nimonic PE 16 Superalloy

K. Bhanu Sankara Rao, V. Seetharaman, S.L. Mannan and P. Rodriguez

Metallurgy Programme, Reactor Research Centre, Kalpakkam Tamil Nadu – 603 102, India

CONTENTS

ISSN 0334-1704

ABSTRACT

The tensile flow and fracture behaviour of a Nimonic PE 16 superalloy has been investigated in the temperature range 300 to 923K and at strain rates varying from 3.2×10^{-5} s^{-1} to 3.2×10^{-2} s^{-1}. Prior to testing, the alloy has been solution annealed at 1313K for 4 h followed by air cooling and then subjected to an intermediate ageing at 1073K for 2 h and a final ageing treatment at 973K for 8 h. The yield strength of the alloy at low strain rates decreases gradually and monotonically with an increase in the test temperature, whereas the yield strength data evaluated at high strain rates show a shallow minimum at 773K. The ductility of the alloy at low strain rates shows minima at 573K and maxima at 673K. In contrast, the ductility data obtained at high strain rates exhibit minima at 773K. Serrated flow occurs in this alloy in the temperature range 523 to 873K and at strain rates lower than 3×10^{-3} s^{-1}. A detailed analysis of the dependence of the critical strain for the onset of serrations on temperature and strain rates yields an apparent activation energy of 240 kJ/mol for serrated flow at temperatures below 673K. Fractography of samples tested up to 573K at low strain rates has revealed predominantly transgranular ductile fracture with some amount of intergranular cracks associated with the decohesion of the $M_{23}C_6$ precipitates. While purely transgranular fracture is observed in the temperature range 673–773K, intergranular fracture dominates at temperatures above 773K. Detailed correlations between the tensile properties and the fractographic features are presented.

1. INTRODUCTION

Nimonic PE 16 superalloy is a wrought nickel-iron base alloy strengthened by solid solution hardening effects of chromium and molybdenum additions and by the precipitation hardening effects of the intermetallic compound, γ' [Ni_3(Al, Ti)]. This alloy combines the high strength of the age hardening nickel base alloys with excellent fabrication characteristics. Apart from its widespread use in gas turbine flame tubes, missile hot components, superheater tubes and aircraft ducting systems /1/, it is also considered as a potential material for core components in liquid sodium cooled fast reactors. In spite of its wide range of applications, the mechanical behaviour of this alloy at elevated temperatures has not been investigated in detail.

In view of the importance of the PE 16 alloy, a detailed study on different aspects of the physical metallurgy of this alloy has been undertaken in our laboratory. As a part of this programme, investigations on the influence of thermomechanical processing /2/, double ageing treatments /3/ and long term exposures at elevated temperatures /4/ on the microstructure and tensile properties of this alloy have already been completed. This paper reports the tensile deformation behaviour and fracture morphology of this alloy at different temperatures (300–923K) and strain rates ($3.2 \times 10^{-5} - 3.2 \times 10^{-2}$ s^{-1}).

2. EXPERIMENTAL PROCEDURE

The Nimonic PE 16 alloy was supplied by Henry Wiggin and Co., Hereford, U.K. in the form of rods of 10 mm in diameter from Heat No. SNJ 2371. The chemical composition of this heat is shown in Table 1. Cylindrical specimens for tensile tests with a gauge

TABLE 1. Chemical Composition of Nimonic PE 16 Alloy

Element	Amount wt%	Element	Amount wt%
C	0.07	Ti	1.2
Si	0.26	Al	1.2
Cu	0.06	Cr	16.5
Mn	0.04	Ni	43.23
Zr	0.03	Co	0.27
S	0.004	Fe	33.28
Mo	3.3	B	0.0015

diameter of 4 mm and a gauge length of 25 mm were machined from these rods in the as-received condition. These samples were solution annealed at 1313K for 4 h and then subjected to double ageing treatments consisting of intermediate ageing at 1073K for 2 h followed by final ageing at 973K for 8 h. Tensile tests were carried out at different temperatures in the range 300 to 923K and at nominal strain rates varying from 3.2×10^{-5} s^{-1} to 3.2×10^{-2} s^{-1} using an Instron Model 1195 universal testing machine. Fractography of the tensile tested samples was carried out using a Philips 501 scanning electron microscope. Thin foils for transmission electron microscopy were prepared by electropolishing in a solution containing 20% perchloric acid and 80% methanol at 10V at temperature below 240K.

3. RESULTS

3.1. Microstructure

Fig. 1 shows the discrete and globular carbide precipitates formed along the grain boundaries after the intermediate ageing treatment at 1073K for 2 h. The electron diffraction pattern clearly demonstrates that these precipitates correspond to the $M_{23}C_6$ type of carbides. This identification was also confirmed by the results of the energy dispersive X-ray microanalysis /3/. On subjecting the alloy to final ageing at 973K

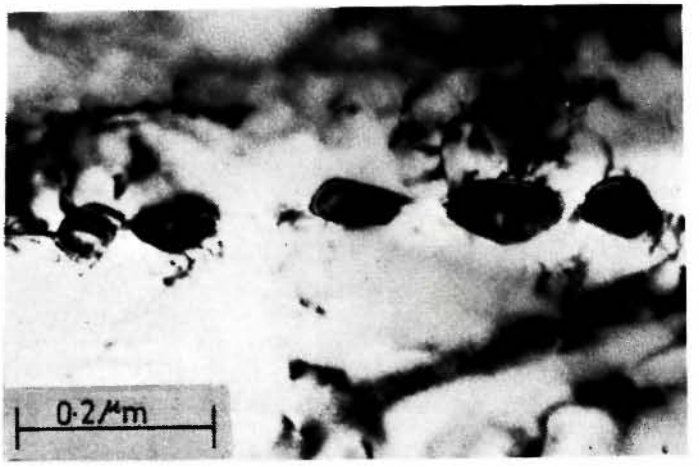

(a)

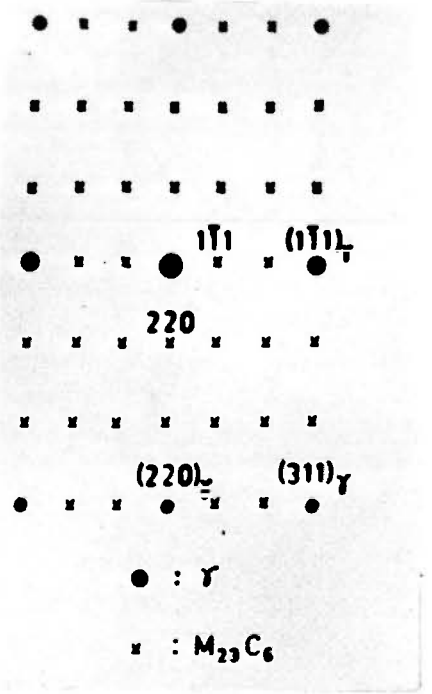

(b)

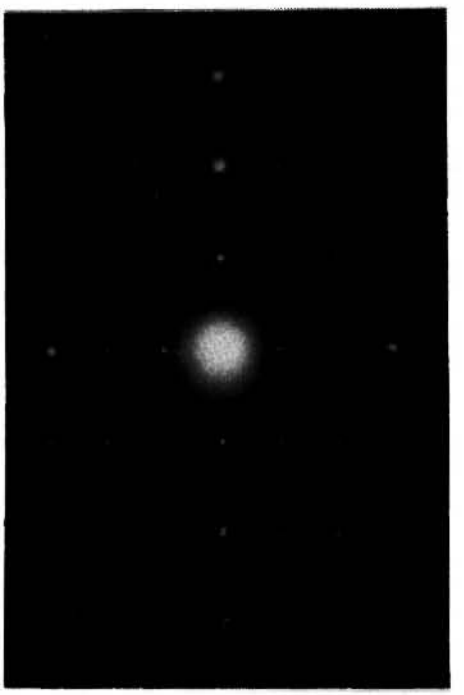

(c)

Fig. 1. (a) Transmission electron micrograph of the sample .ged at 1073 K for 2 h. Discrete carbides along the grain boundaries are seen; (b) and (c) are the selected area diffraction patterns and the key taken from the region corresponding to (a).

for 8 h, spherical and coherent γ' precipitates with a mean radius of 8 nm were found to precipitate uniformly throughout the matrix (Fig. 2). In addition, intergranular precipitation of carbides was found to continue during final ageing too, resulting in a nearly continuous network of $M_{23}C_6$ carbides along the grain boundaries, as illustrated in Fig. 3.

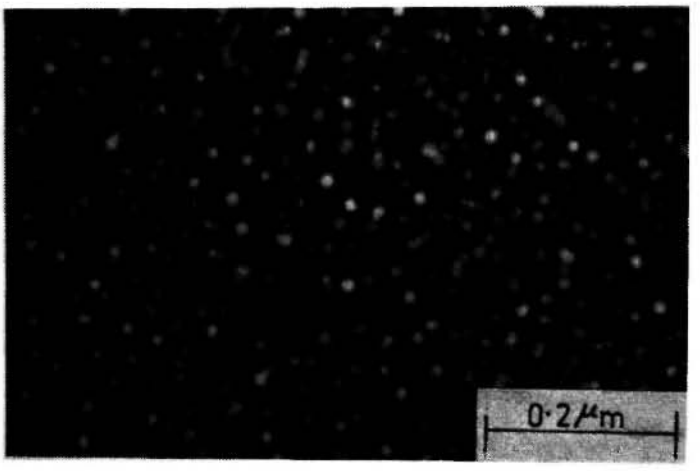

Fig. 2. Dark field micrograph taken from a (210) γ', reflection showing spherical γ' precipitates distributed uniformly throughout the matrix.

Fig. 3. Large $M_{23}C_6$ precipitates formed after final ageing at 973 K for 8 h.

3.2. Tensile Properties

Figures 4–7 show the variation of tensile properties such as yield strength, ultimate tensile strength, total elongation and reduction in area evaluated at different temperatures and strain rates. At very high strain rates (3.2×10^{-2} s^{-1}) the yield strength of the alloy decreases with an increase in the test temperature, reaches a minimum at about 773K and thereafter increases marginally up to about 923K. This type of temperature dependence of yield strength is also seen at the strain rates of 3.2×10^{-3} and 3.2×10^{-4} s^{-1}. However, at the lowest strain rate, (3.2×10^{-5} s^{-1}), the yield strength vs. temperature plot exhibits plateau in

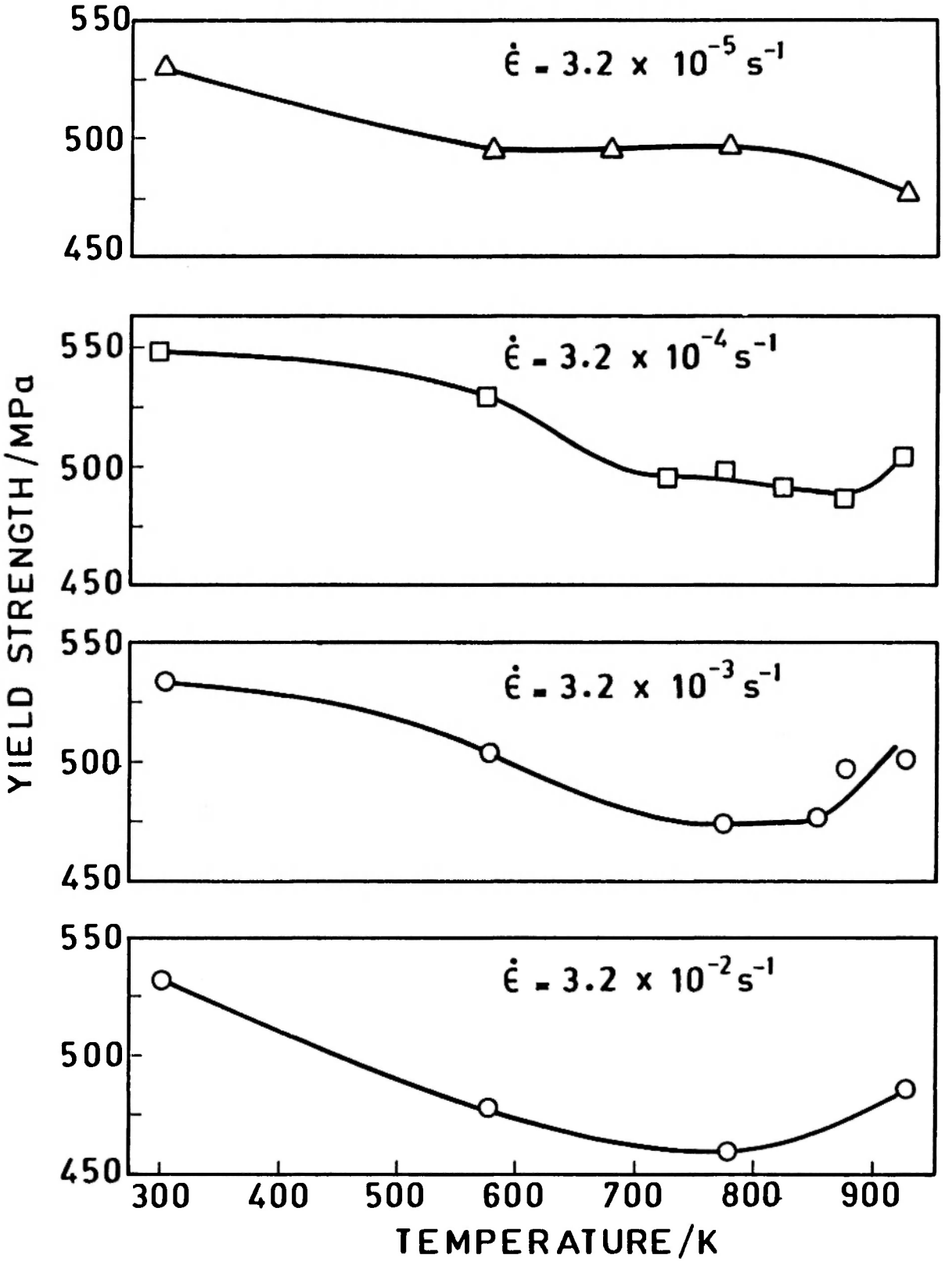

Fig. 4. Variation of the yield strength of the samples subjected to final ageing at 973 K for 8 h as a function of the test temperature and strain rate.

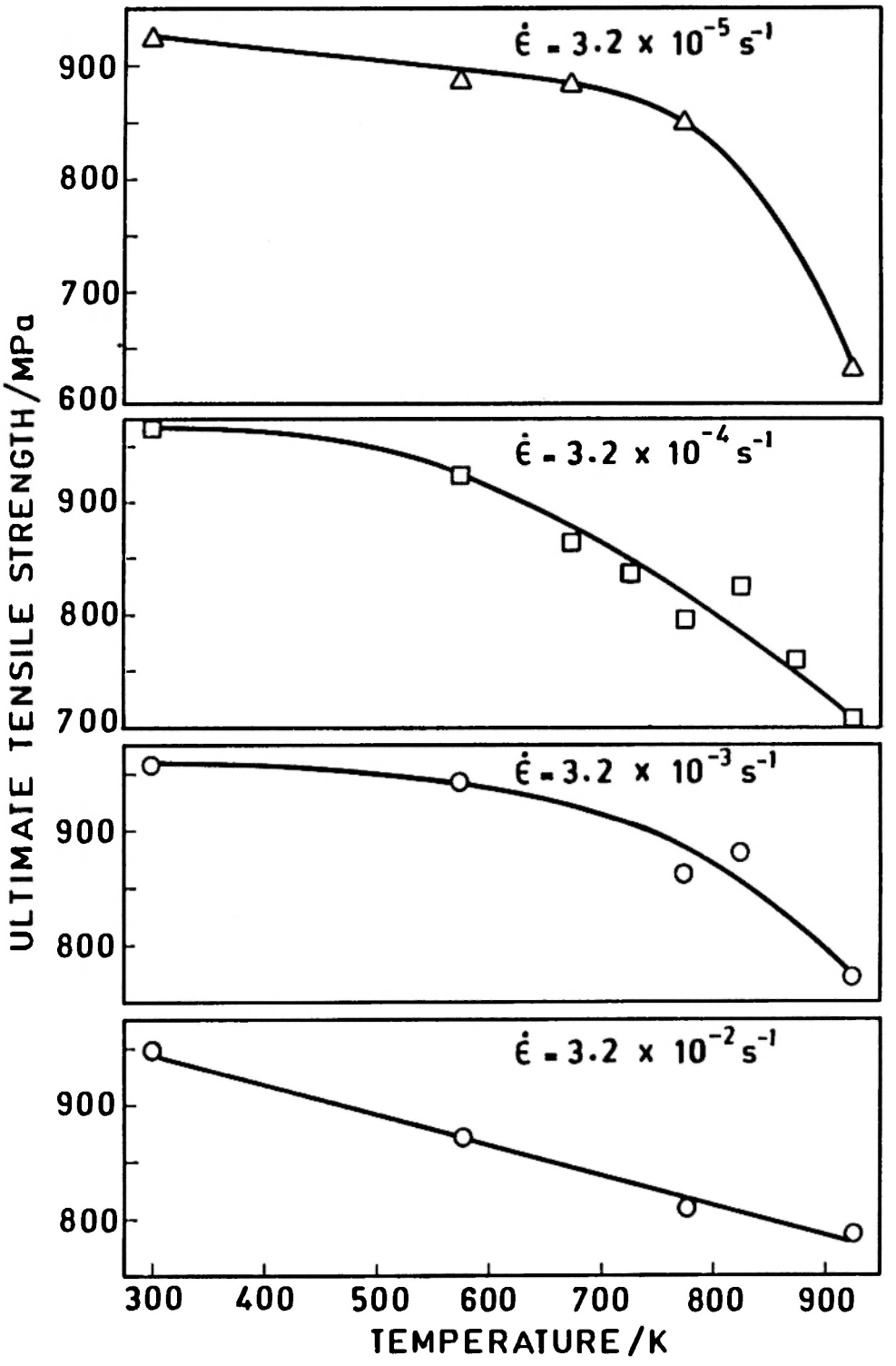

Fig. 5. Variation of the ultimate tensile strength with test temperature and strain rate.

the range 573–823K. In general, the rate of decrease of yield strength with temperature (at low test temperatures) is found to increase with an increase in the strain rate. Furthermore, the yield strength of the alloy at the lowest strain rate used, viz. $3.2 \times 10^{-5}\ s^{-1}$ decreases beyond 773K. The ultimate tensile strength of the alloy decreases with an increase in the test temperature at all the strain rates employed (Fig. 5). The

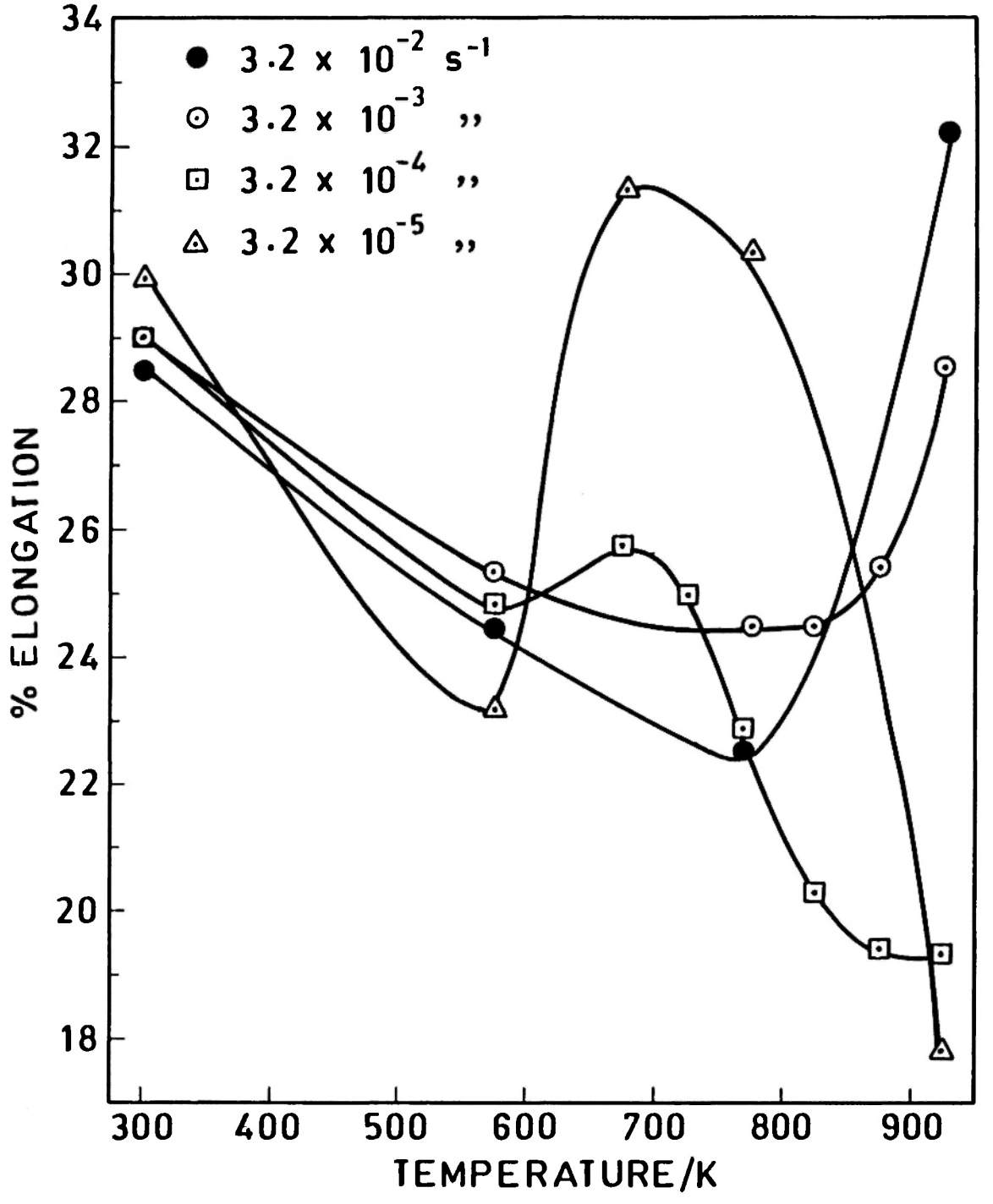

Fig. 6. Variation of the total elongation with test temperature and strain rate.

temperature dependence of the ultimate tensile strength at a strain rate of 3.2×10^{-2} s^{-1} is nearly linear. In contrast, the U.T.S. evaluated at low strain rates changes very gradually with temperature up to about 773K and thereafter decreases very sharply.

The ductility of the alloy shows a complex type of dependence on both the test temperature and strain rate. For example, the percentage elongation values (Fig. 6) measured at strain rates less than 3.2×10^{-4} s^{-1} exhibit minima at 573K and maxima at 673K, whereas those measured at strain rates higher than 3×10^{-3} s^{-1} show well-defined minima at 773K.

These trends are also reflected in the variation of the reduction in area with the test temperature (Fig. 7) particularly at low strain rates.

The macroscopic work hardening rate, θ for different specimens was computed using the following expression:

$$\theta = \frac{\sigma_{0.02} - \sigma_{0.002}}{0.018} \quad (1)$$

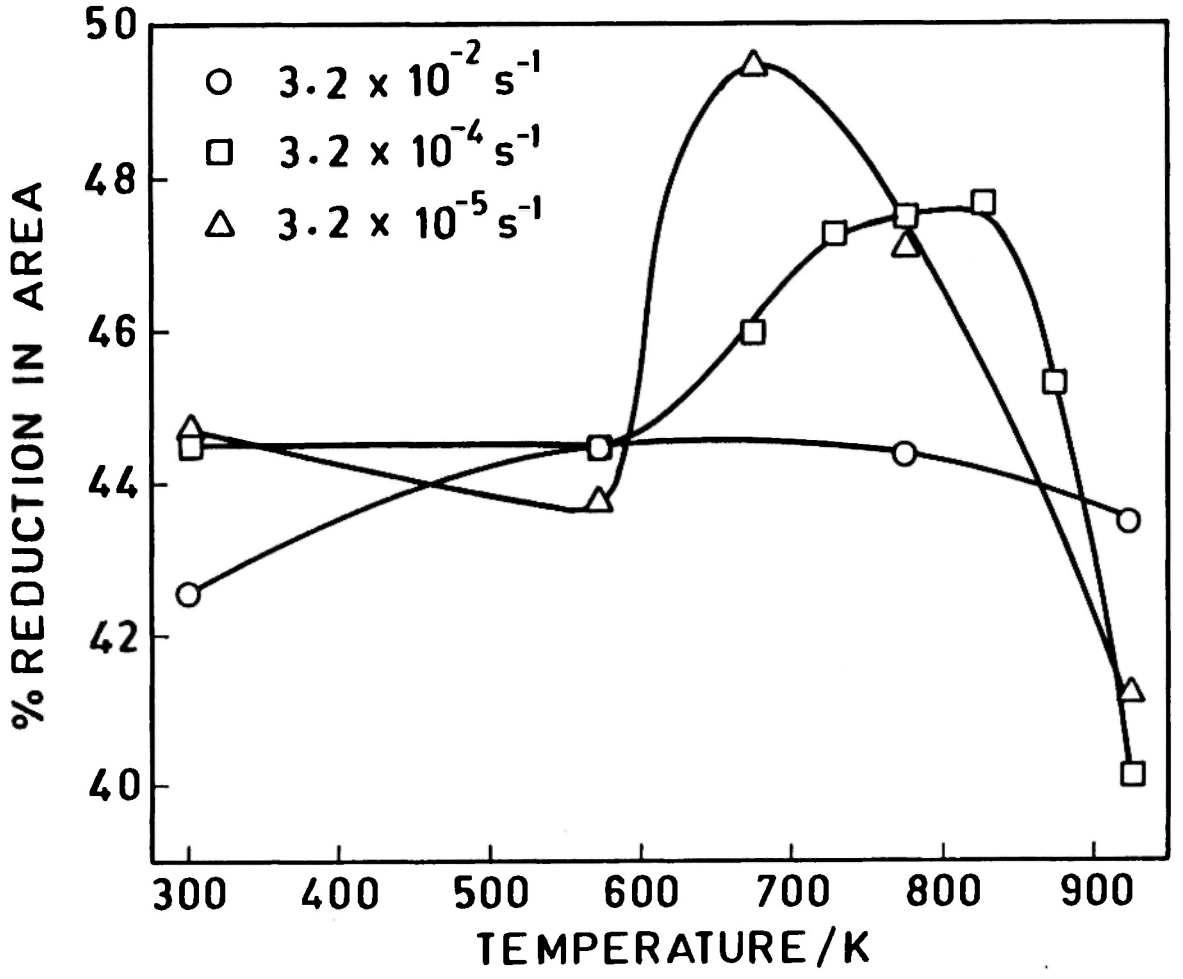

Fig. 7. Variation of the reduction in area with test temperature and strain rate.

where $\sigma_{0.02}$ and $\sigma_{0.002}$ refer to the true stress values corresponding to the plastic strain levels of 0.02 and 0.002, respectively. Table 2 shows the variation of θ with test temperature and strain rate. It can be seen that the work hardening rate increases markedly with a decrease in the strain rate only at 773K. At other temperatures, the variation of θ with the imposed strain rates is quite small. This temperature (773K) nearly coincides with the upper temperature limit of the yield strength plateau at a strain rate of 3×10^{-5} s^{-1}.

TABLE 2. Variation of Work Hardening Rate, $\theta = \frac{\sigma_{0.02} - \sigma_{0.002}}{0.018}$ / MPa with Strain Rate and Test Temperature

Temp. (K) / Strain rate (s^{-1})	300	573	773	923
3×10^{-2}	7.1×10^3	7.2×10^3	5.5×10^3	6.4×10^3
3×10^{-4}	6.1×10^3	–	8.3×10^3	6.7×10^3
3×10^{-5}	6.1×10^3	6.3×10^3	11.1×10^3	6.1×10^3

3.3. Serrated Flow

The tensile flow curves obtained in the temperature range 523 to 873K at strain rates lower than 3.2×10^{-3} s^{-1} exhibited different types of serrations. These serrations can be classified into types A, B or C on the basis of the classification scheme proposed by Brindley and Worthington /5/. The serrations observed at 523K can be characterised as a mixture of type A and B. Fig. 8, which shows a typical load elongation

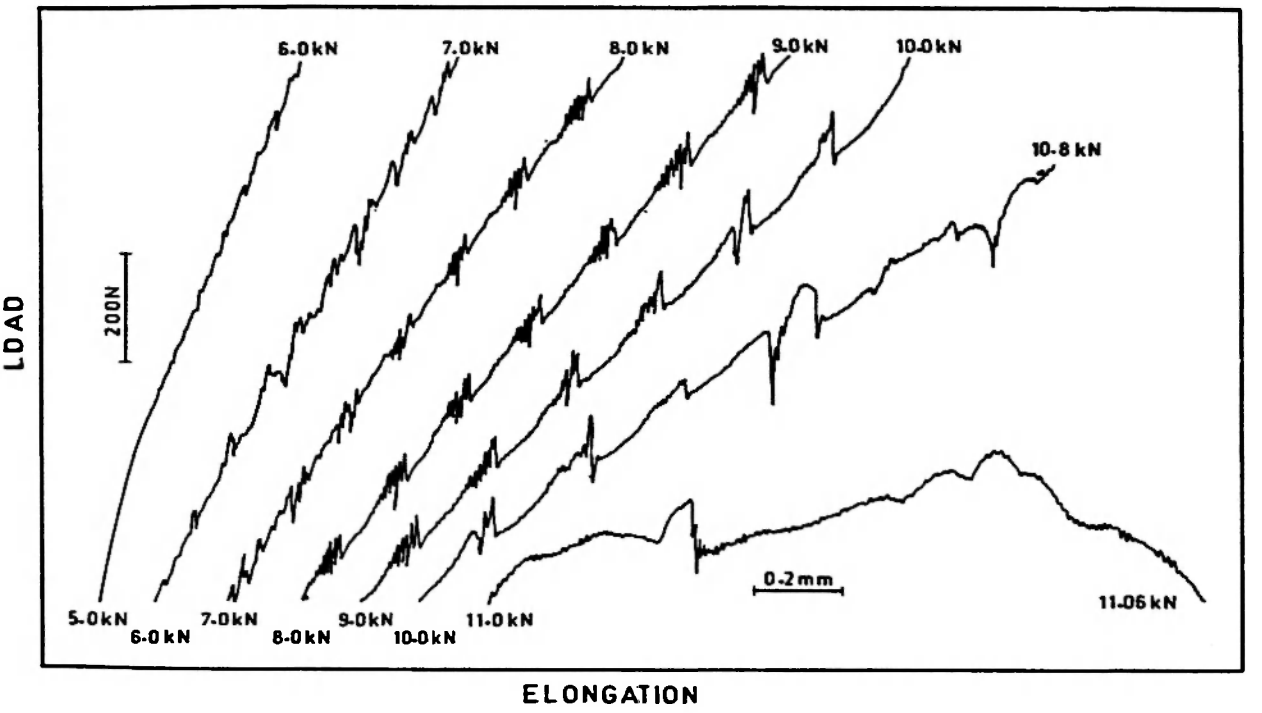

Fig. 8. Load-elongation plot for the sample tested at 523 K at a strain rate of 3.2×10^{-5} s^{-1}.

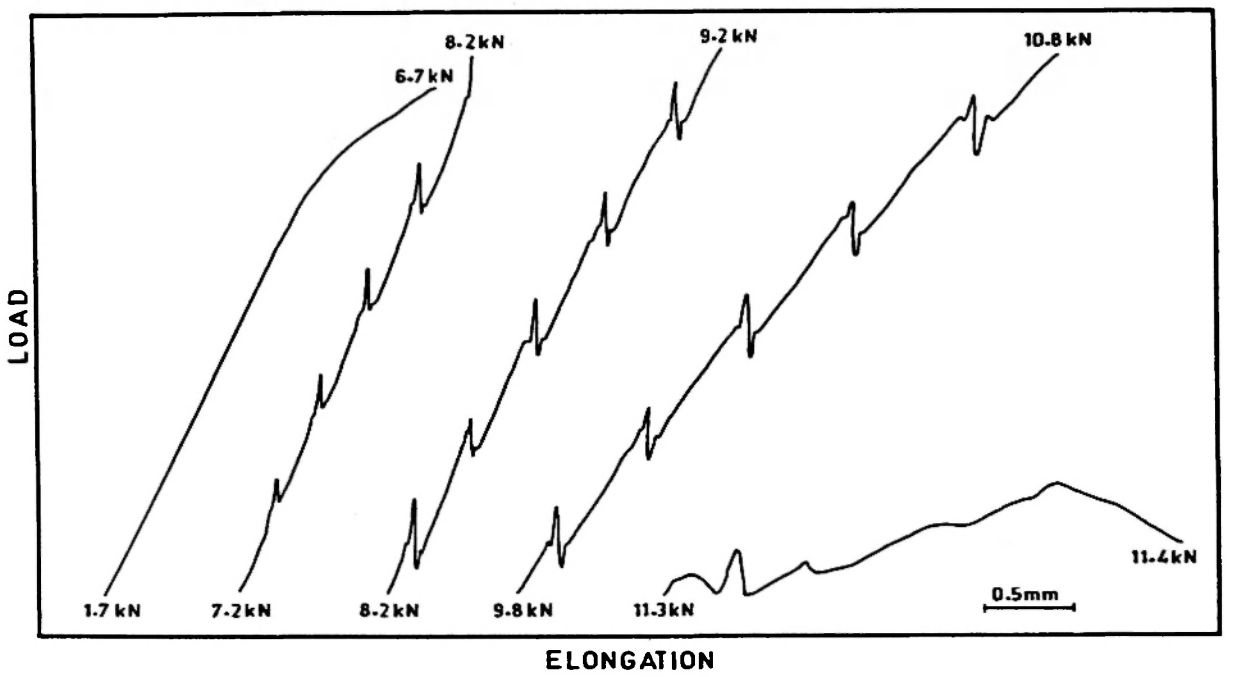

Fig. 9. Load-elongation plot obtained on testing at a strain rate of 3.2×10^{-3} s^{-1} and at 573 K.

curve obtained at this temperature, illustrates the above observations. In the temperature range $573 \leqslant T < 673K$, the characteristics of the serrations observed are found to be strongly dependent on the imposed strain rate. At low strain rates (3.2×10^{-5} s^{-1}) the serrations were a mixture of types A + B while at high strain rates (3.2×10^{-3} s^{-1}) the serrations were mainly of type A. Fig. 9 clearly reveals type A serrations observed at 573K and at a strain rate of 3.2×10^{-3} s^{-1}. It can also be seen that the period between successive serrations increases with an increase in plastic strain. Type C serrations were found to occur at or above 673K at the lowest strain rate employed (Fig. 10). However, as the imposed strain rate increases, the onset of type C serrations occurs at progressively higher temperatures. At any given strain rate, the magnitude of stress drop $\Delta\sigma$ is found to increase with an increase in the test temperature, irrespective of the type of serrations observed (Table 3). Similarly, $\Delta\sigma$ is found to increase with a decrease in the applied strain rate at a constant test temperature. All the above mentioned characteristics of serrated flow are in good agreement with the results published by Chickering *et al.* /6/.

The serrations are observed only after the specimens have been deformed beyond a critical strain, ϵ_c. The strain rate dependences of the critical strain, ϵ_c at 573 and 823K are shown in Fig. 11 (a) and (b), respectively. It can be seen that the critical strain decreases with a decrease in the applied strain rate at both these temperatures. Critical strain values corresponding to the serrations of Type A or A + B observed in the low temperature regime are found to decrease with an increase in the test temperature. In contrast, an 'inverse' temperature dependence of

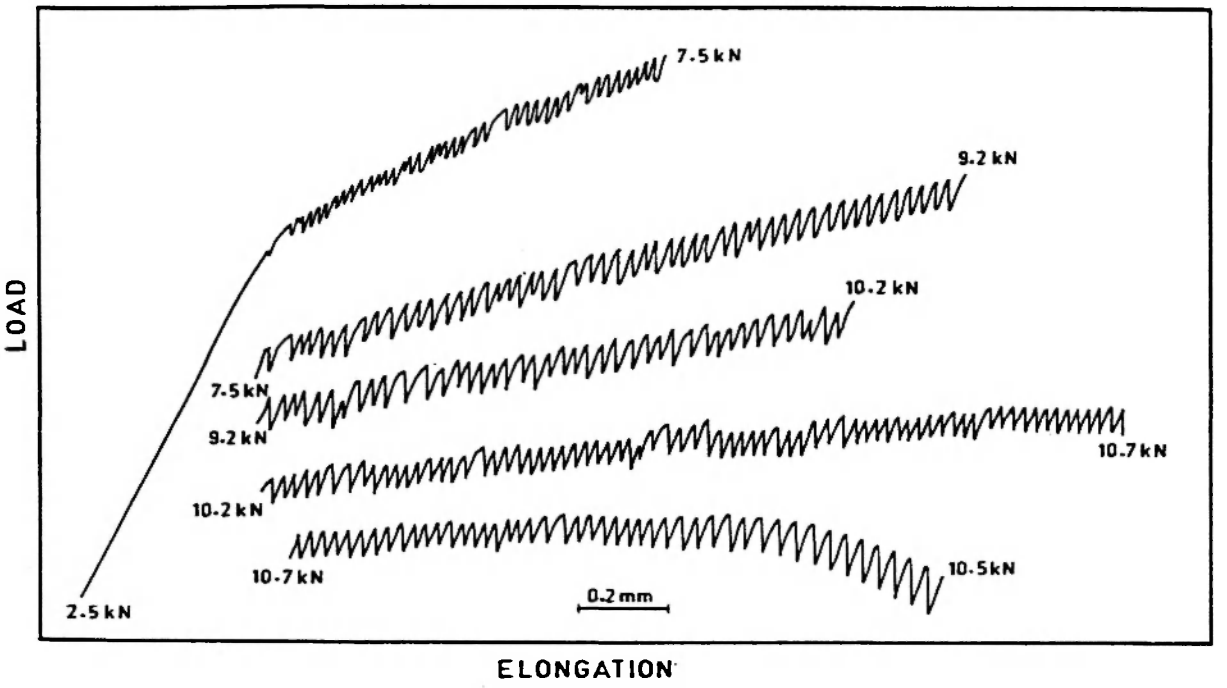

Fig. 10. Load-elongation plot obtained on testing at 673 K and at a strain rate of 3.2×10^{-5} s^{-1}. Type C serrations are clearly visible.

TABLE 3. Details of Serrated Flow Observed at Different Temperatures (T) and Strain Rates ($\dot{\epsilon}$)

$\dot{\epsilon}$ (s^{-1})	T (K)	Type of serrations	Stress drop, $\Delta\sigma^*$ (MPa)
	573	A	12
	623	A+B	13
3×10^{-4}	673	A+B	16
	723	B	21
	773	C	24
3.2×10^{-3}		A	8
1.3×10^{-3}		A	11
6.7×10^{-4}	673	A+B	14
1.3×10^{-4}		A+B	16

* Stress drop values correspond to a plastic strain of 0.1.

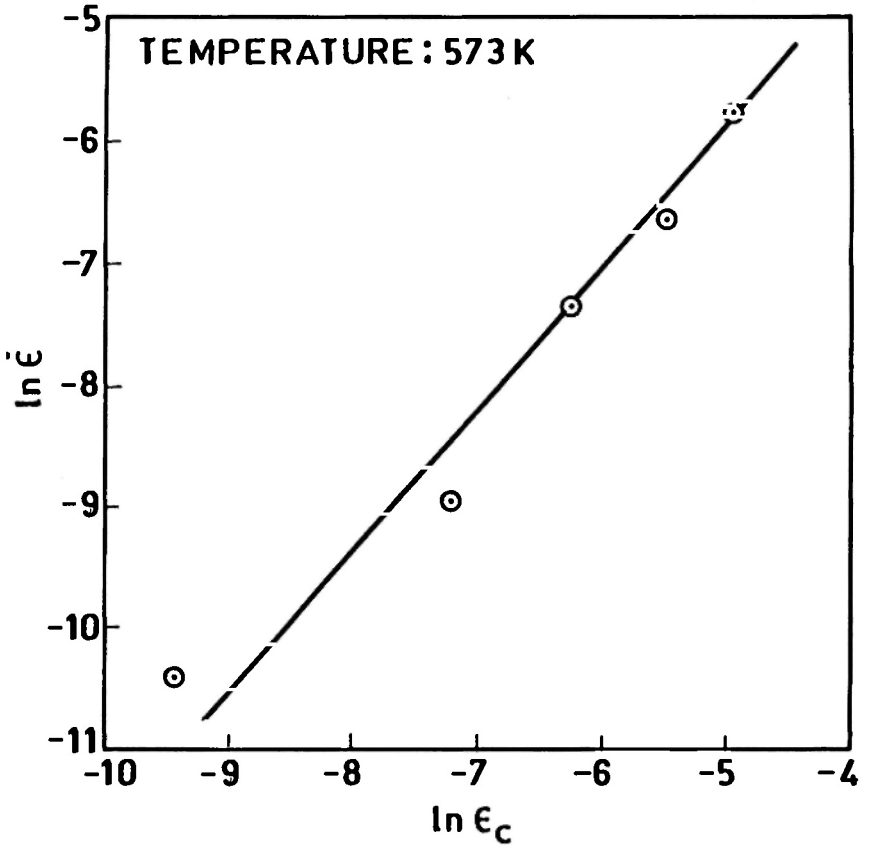

Fig.11 (a)

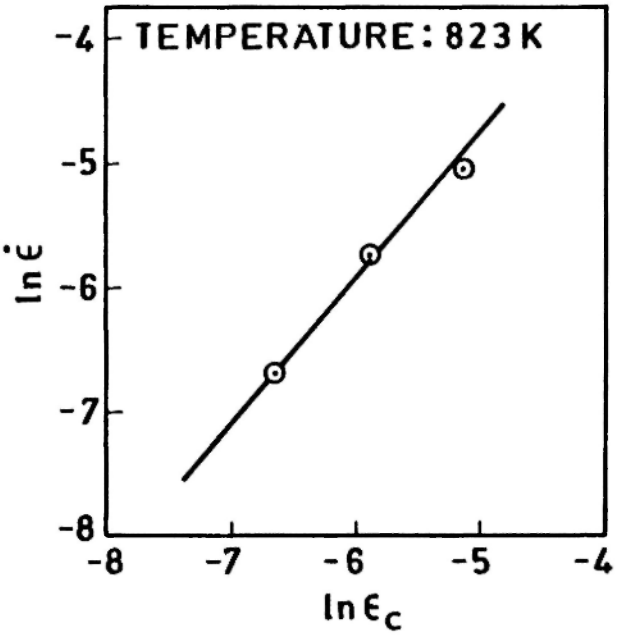

Fig.11 (b)

Fig. 11. Variation of the critical strain, ϵ_c with the imposed strain rate, $\dot{\epsilon}$, at (a) 573 K and (b) 823 K.

ϵ_c is observed at high temperatures where type C serrations are encountered. Fig. 12 (a) and (b) illustrate both these observations.

It is possible to determine the apparent activation energy Q associated with the serrated yielding process using the following equation /5, 7/:

$$\dot{\epsilon} = A\epsilon_c^{(m+\beta)} \exp^{(-Q/kT)} \quad (2)$$

where A, m and β are constants, T is the temperature, ϵ is the strain rate and k is the Boltzmann constant. The plots of $\ln\epsilon_c$ vs. $\ln\dot{\epsilon}$ shown in Fig. 11 yield values of $(m + \beta)$ as $\sim$ 1.2 at 573 and 823K. Estimation of the activation energy Q from the plots of $\ln\epsilon_c$ vs. 1/T is restricted to the low temperature regime ($T \leqslant$ 623K) where positive Portevin-LeChatelier effect is noticed. This yields an activation energy value of 240 kJ mol^{-1} for type A/A + B serrations occurring at test temperatures below 623K.

3.4. *Fracture Behaviour*

Fractographic analysis of the samples tested at different temperatures and strain rates in general, shows a mixed mode of fracture. Figures 13 and 14 illustrate the observations made on samples tested at two specific strain rates of 3×10^{-5} s^{-1} and 3×10^{-2} s^{-1} respectively. Tensile deformation at 300 and 573K at both the strain rates leads to the formation of several intergranular cracks, even though the interior portions of the grains exhibit large dimples resulting from the coalescence of microvoids – a characteristic feature of ductile fracture [Fig. 13 (a) and Fig. 14 (a)]. Similar fractographs showing a large number of dimples along with a limited amount of coarse intergranular cracks are also obtained on testing at 3×10^{-2} s^{-1} and at 773K [Fig. 14(b)]. In contrast, the fracture surfaces obtained on testing in the temperature range 673–773K and at a strain rate of 3×10^{-5} s^{-1} reveal evidence for the occurrence of pure ductile fracture [Fig. 13(b)]. Similar fracture characteristics are also observed in samples tested at 923K and at a strain rate of 3×10^{-2} s^{-1} [Fig. 14(c)]. However, the tensile fracture surfaces produced on testing at 923K and at 3×10^{-5} s^{-1} are predominantly intergranular, revealing extensive wedge cracks along the triple points [Fig. 13(c)].

4. DISCUSSION

4.1. *Tensile Properties*

The temperature dependence of the flow stress of alloys hardened by the γ' precipitates has been studied by several investigators including Copley and Kear /8, 9/, Stoloff and Davies /10/ and Beardmore *et al.* /11/. These results have been reviewed by Stoloff /12/ and by Pope and Ezz /13/. In general, the flow stress of the alloy containing a mixture of γ and γ' exhibits different types of temperature dependence depending on the volume fraction, f of γ'. Alloys containing a high volume fraction of γ' (e.g. Mar-M-200 alloy and Nimonic 115, f = 0.06) are characterised by an increase in flow stress with temperature, while those containing low volume fraction of γ' (e.g. Inconel X-750, f = 0.14) exhibit negative temperature coefficients of flow stress. The most widely accepted mechanism for the anomalous temperature dependence of flow stress for $\gamma'[Ni_3(Al, Ti)]$ and for alloys containing a high volume fraction of γ' involves cross slip of screw dislocations from (111) planes where they are mobile to (010) planes where they become immobile /13/. The driving force for the (111) to (010) cross slip is provided both by the anisotropy of the antiphase boundary energy and by the resolved shear stress on (010) (101).

The decrease in flow stress of the PE 16 alloy (f = 0.12) with an increase in test temperature in the range 300 to 573K is consistent with the mechanical behaviour reported in alloys containing a low volume fraction of γ'. In the intermediate temperature range, the rate of decrease of yield strength with temperature diminishes. This leads to well defined yield strength plateaus at low strain rates (Fig. 4). It can be seen that the temperature corresponding to the start of the yield stress plateau increases with an increase in the strain rate. Furthermore, this temperature range coincides with that corresponding to pronounced occurrence of serrated flow.

Enhanced work hardening rates observed at 773K at strain rates of 3×10^{-5} s^{-1} and 3×10^{-4} s^{-1} (Table 2) can also be attributed to the phenomenon of serrated flow resulting from dynamic strain ageing. Similar correlations between dynamic strain ageing, flow stress plateaus and high work hardening rates have been

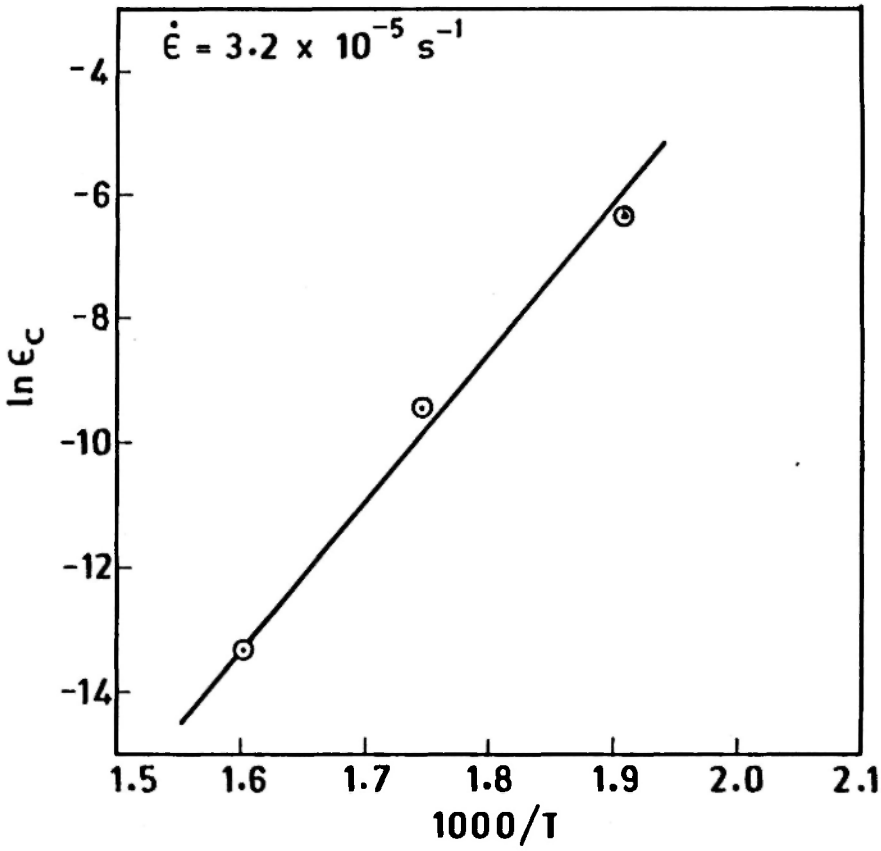

Fig.12 (a)

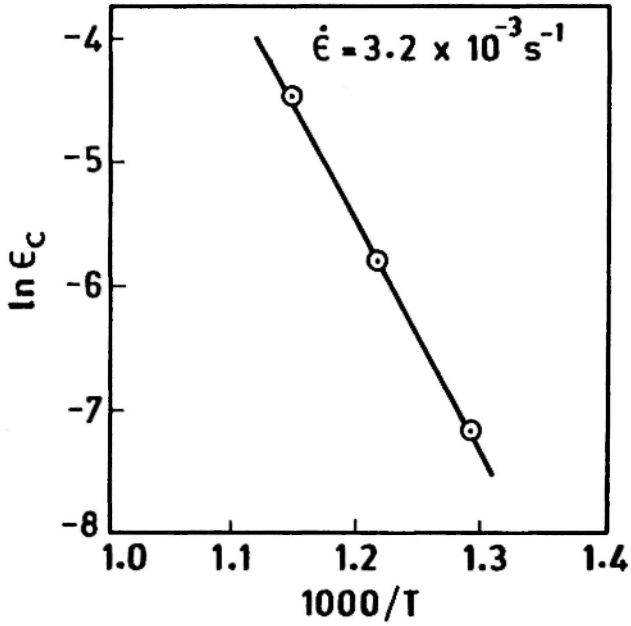

Fig.12(b)

Fig. 12. Variation of the critical strain, ϵ_c with the test temperature. While the plot in (a) shows normal temperature dependence of ϵ_c for type A/A+B serrations occurring at low temperatures, the plot shown in (b) indicates inverse temperature dependence of ϵ_c for type C serrations occurring at $T \geqslant 673$ K.

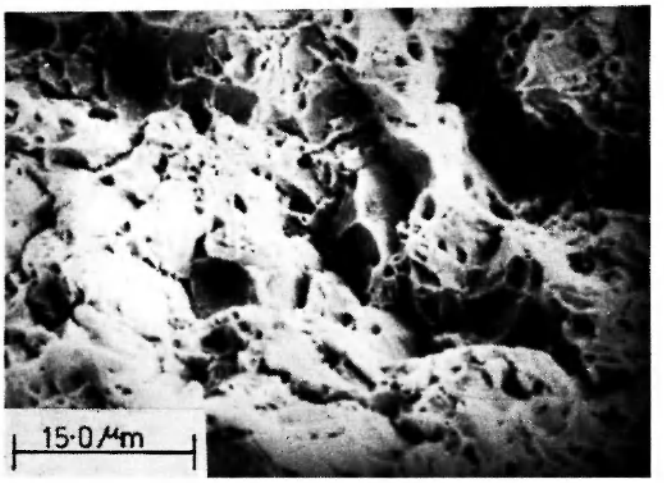

(a)

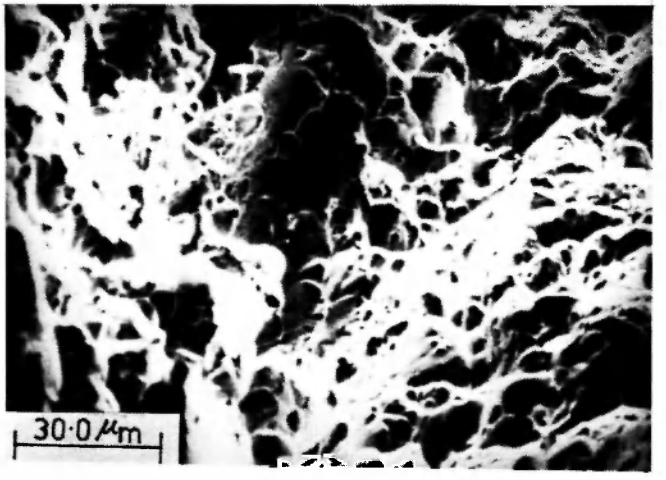

(b)

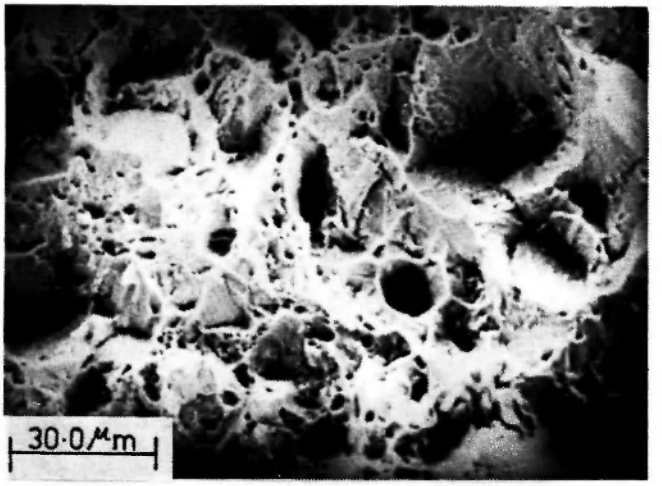

(c)

Fig. 13. Scanning electron micrographs of the fracture surfaces of the samples tested at a strain rate of 3.2×10^{-5} s^{-1} and at (a) 300 K (b) 773 K and (c) 923 K.

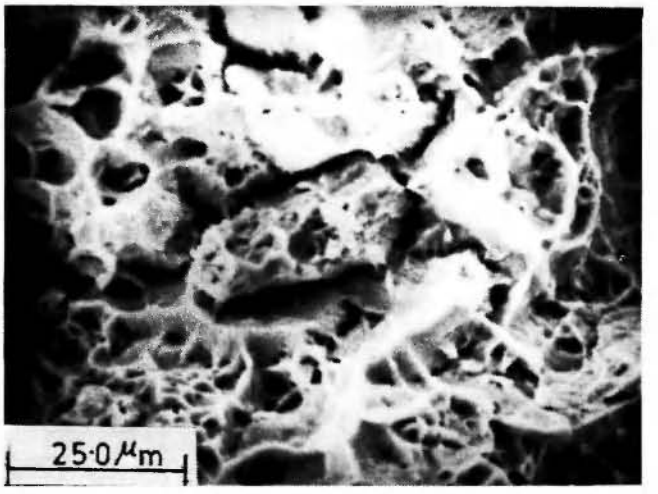

(a)

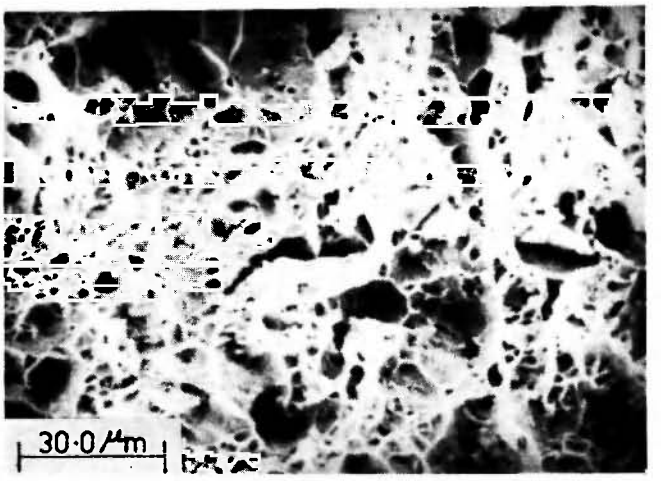

(b)

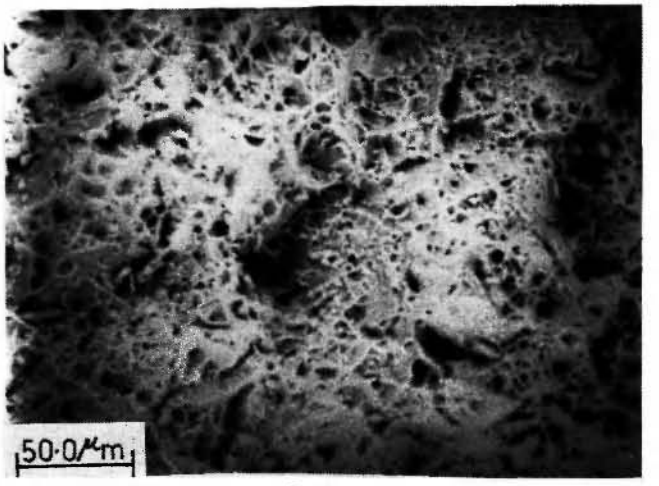

(c)

Fig. 14. Scanning electron micrographs of the fracture surfaces of the samples tested at a strain rate of 3.2×10^{-2} s^{-1} and at (a) 300 K (b) 773 K and (c) 923 K.

reported by Barnby /14/, Michael *et al.* /15/, Kutumba Rao *et al.* /16/ and Mannan *et al.* /7/. The increase in the work hardening rate within the dynamic strain ageing regime is considered to be due to an increase in the rate of accumulation of dislocations /17/.

The increase in yield strength with test temperature ($d\sigma y/dT \geqslant 0$) observed near 923K and at strain rates higher than 3.2×10^{-4} s^{-1} can be attributed to an increase in the antiphase boundary energy leading to enhanced order hardening effects. In contrast, the yield strength value of the alloy measured at 923K and at a strain rate of 3×10^{-5} s^{-1} is significantly lower than the evaluated at 773K. This may be due to any one of the following reasons: (i) Softening due to dynamic coarsening of the γ' precipitates during testing, (ii) Softening due to the operation of dynamic recovery processes and (iii) Onset of microcracking mainly along the grain boundaries. The first process, namely dynamic coarsening of the γ' precipitates during testing should lead to an increase in the tensile work hardening rate. On the other hand, Table 2 clearly shows that the average work hardening rate, θ, decreases sharply above a test temperature of 773K. Furthermore, since the alloy has been aged for a duration (8 h) which is slightly shorter than that corresponding to peak ageing, any coarsening of γ' during initial stages of plastic deformation would only lead to an enhancement in the yield strength. Thus one can rule out dynamic coarsening of γ' as a possible mechanism for the observed reduction in yield strength at 923K at the lowest strain rate. The observation of low tensile ductility at 923K also suggests that dynamic recovery processes could not be responsible for the reduction in the yield strength at this temperature. Thus the occurrence of intergranular cracking processes during early stages of deformation appears to be responsible for the reduced flow stress and poor ductility observed at 923K.

Fig. 6 shows that the samples tested at low strain rates exhibit low values of tensile ductility at 573K and pronounced ductility maxima at 673K. Beyond this temperature a rapid decrease in ductility with an increase in temperature up to 923K is noticed. In contrast, tests carried out at high strain rates lead to clear ductility minima at $\sim$ 773K. It should be pointed out that the flow curves obtained at low strain rates reveal type A/(A + B) serrations and type C serrations at 573 and 673K, respectively. These results appear to indicate that the ductility maxima occurring at 673K are associated with the onset of type C serrations. This observation is contradictory to those reported by Koch and Troiano /18/ and Barnby /14/. On the other hand, De Almeida and Monterio /19/ have reported that type 316 austenitic stainless steel tends to maintain a fairly high level of ductility in the dynamic strain ageing regime. It is therefore imperative to consider mechanisms other than dynamic strain ageing which could affect the ductility of the PE 16 alloys.

Fractographs obtained from samples tested at temperatures below 573K reveal several intergranular cracks along with the dimples characteristic of the microvoid coalescence in the grain interior. The formation of intergranular cracks during deformation at such low temperatures may appear surprising. But this is not so, if one considers the fact that the grain boundaries are decorated with a high density of discrete carbide precipitates ($M_{23}C_6$). During plastic deformation when slip bands propagate and impinge on an intergranular carbide precipitate, microcracks can develop at the interface between the carbide and the matrix. Indeed, careful studies carried out by Shiozawa and Weertman /20/ on Astraloy show that microcracking occurs after a plastic strain as low as 0.015 at 300K and that microcracks are invariably associated with slip steps. Moreover, it has been postulated that if such samples, after pre-straining at room temperature, are heated at 1000K for short durations, then the tensile residual stresses drive vacancies into microcracks to produce voids on boundaries parallel to the direction of maximum principal stress /21/. This has been verified by Dyson *et al.* /22/ and by Nazmy and Duerig /23/ in the course of their experiments in several wrought and cast nickel base alloys.

Mills /24/ has observed the intergranular dimple rupture network in Inconel X-750 samples fractured at 300K and attributes it to the localised deformation and the coalescence of microvoids along the grain boundary γ' denuded zones. He has also reported that a transition from intergranular to transgranular mode of fracture occurs in the intermediate range of temperatures (590–700K) and that pure transgranular fracture occurs in the range 920–977K. It should be clarified that no γ' denuded zone along the grain boundaries was identified in the PE 16 alloy samples examined in this work. Therefore, the microcracking observed along the austenite grain boundaries can only be attributed to the decohesion of the interface between the $M_{23}C_6$ particles and the matrix due to the stress concentration effects resulting from the impingement of slip bands on the intergranular carbide precipitates. At low strain rates and intermediate tem-

peratures, the enhanced dislocation activity in the grain interior helps to relieve the stress concentration effects mentioned above, thereby preventing the formation of intergranular cracks. Indeed the fractographs [Fig. 13(b)] corresponding to the samples tested at 673K at a strain rate of 3×10^{-5} s^{-1} reveal evidence of fully ductile fracture free from any intergranular cracks. This also leads to an improvement in ductility as evidenced by the ductility maximum seen at 673K at low strain rates. The recovery in ductility observed above 773K during testing at high strain rates can also be attributed to the reduction in the stress concentration effects due to the operation of the processes mentioned above.

4.2. *Dynamic Strain Ageing*

Serrated yielding has been reported in several nickel/iron base superalloys and austenitic stainless steels over a wide range of temperatures and strain rates. This phenomenon has been widely attributed to dynamic strain ageing (DSA) of dislocations by either substitutional or interstitial solutes. The effects of DSA and the mechanisms proposed for DSA have been reviewed critically by Hall /25/, Brindley and Worthington /5/, Baird /26/, Rodriguez /27/ and by McCormick /28, 29/. Recent studies by Mulford /30/ and Hayes and Hayes /31/ have focussed attention on the specific roles of γ' and carbide precipitates in the serrated flow behaviour of precipitation hardenable alloys.

It has already been stated in Section 3.3 that the apparent activation energy for the serrated flow process occurring in the low temperature regime ($T \leqslant 623K$) is 240 kJ mol^{-1}. This value is in good agreement with the results of Jenkins and Smith /32/, Tamhankar *et al.* /33/ and Mannan *et al.* /7/ obtained in Fe-Ni-Cr, Fe-Ni-Cr-Mn-C and type 316 stainless steel, respectively. It should also be noticed that the activation energy of 240 kJ mol^{-1} compares favourably with the activation energy for the bulk diffusion of substitutional solutes in the γ phase of nickel base alloys (Q_{Al} = 270 kJ/mol, Q_{Ti} = 257 kJ/mol) /34/. This suggests that the type A/A+B serrations occurring at temperatures below 623K are due to the locking of dislocations by the substitutional solutes. In this context, it is relevant to state that the activation energy values for serrated flow in precipitation hardenable alloys can vary over a wide range depending on the prior heat treatments, although the mechanism for dynamic strain ageing may remain the same /31/. This is due to the fact that changes in the volume fraction and mean size of the γ' precipitates brought about by different heat treatments can lead to changes in the net concentration of the solute in the matrix which, in turn, alters the critical strain values for the onset of serrations. One should, therefore, be cautious in comparing the activation energy values for serrated flow obtained in different investigations for determining the mechanism of DSA. Although Chickering *et al.* /6/ have attributed the serrated flow occurring in the PE 16 alloy at low temperatures to the interaction of dislocations with carbon-vacancy pairs or with substitutional solutes, the present work demonstrates that it is only due to the interaction between the dislocations and substitutional solutes.

Type C serrations occurring at temperatures above 623K could have formed due to the following two reasons: (i) Dynamic strain ageing effects resulting from the unlocking of dislocations from the atmospheres of substitutional solutes; (ii) repeated shearing of the γ' precipitates by dislocations moving on the same slip plane. The former view is supported by the result published by Koul and Pickering /35/ and also the results reported in Fe-Ni-Cr alloys /32/ while the latter opinion is advanced by Doi and Shimanuki /36/ on the basis of their work on Udimet 520 alloy. In order to resolve this controversy, the deformation behaviour of solution treated samples was studied at a temperature of 773K and at a strain rate of 3×10^{-5} s^{-1}. The results showed that well developed type C serrations with the magnitude of stress drop varying in the range 13 to 27 MPa were observed throughout the stress-strain curve. It may be argued that these serrations could be a result of dynamic precipitation of fine γ' during testing. This can be negated by the fact that the test temperature of 773K is too low to cause dynamic precipitation of γ' in the PE 16 alloy within the test duration. Furthermore, transmission electron microscopy of this sample failed to reveal any evidence for the precipitation of γ' during testing. Besides, if repeated shearing of γ' precipitates in a slip plane causes serrated flow, then these serrations should persist up to fairly high temperatures. Conversely, type C serrations were found to disappear above a test temperature of $\sim$ 873K over a wide range of strain rates. All this evidence conclusively proves that the type C serrations observed in the temperature range 673–873K were not directly related to the shearing of the γ' precipitates by mobile dislocations.

It should be pointed out that the type C serrations occurring at temperatures higher than 673K are characterised by an inverse Portevin-LeChatelier (P-L) effect,

i.e. ϵ_c increases with an increase in the test temperature. Although the mechanisms leading to inverse PL effect are not well understood, it is generally agreed that the onset of serrated yielding in this regime is caused by the unlocking of dislocations from the already existing atmospheres of solute atoms /27-29/. However, in the absence of a suitable model for rationalising the dynamic strain behaviour in this range of temperatures and strain rates, it has not been possible to calculate the activation energy associated with type C serrations.

5. CONCLUSIONS

(a) The dependence of yield strength of the PE 16 alloy on the strain rate and test temperature was found to be quite complex. At low strain rates, yield strength plateaus were observed in the temperature range 573 to 823K. These have been explained on the basis of dynamic strain ageing. At high strain rates, the yield strength vs. temperature plots exhibited minima at 773K.

(b) The ultimate tensile strength of the alloy decreases with an increase in the test temperature up to 923K at all the strain rates used.

(c) The maximum value of tensile ductility of the PE 16 alloy occurs at 673K at strain rates less than 3×10^{-4} s^{-1}.

(d) At test temperatures below 673K, the flow curves exhibited type A/A+B serrations depending on the strain rate used. Low strain rates were found to promote the appearance of type A+B serrations while high strain rates lead to the formation of type A serrations only. At test temperatures above 673K, only type C serrations were observed.

(e) The apparent activation energy associated with the type A/A+B serrations occurring at temperatures below 673K was found to be 240 kJ mol^{-1}.

(f) Tensile fracture occurring at test temperatures below 573K can be attributed to the formation of intergranular cracks due to the decohesion of the grain boundary carbides. Fracture surfaces obtained on testing in the temperature range 673–773K revealed predominantly ductile fracture. However, tests conducted at 923K and at very low strain rates showed mixed mode fracture dominated by intergranular wedge cracking.

ACKNOWLEDGEMENTS

The authors wish to acknowledge the cooperation and assistance provided by Mr. S. Vaidyanathan and Miss R. Sandhya.

REFERENCES

1. Nimonic Alloy PE 16, Publication No. 3349 (Henry Wiggin and Co., Hereford, 1976).
2. BHANU SANKARA RAO, K., SEETHARAMAN, V., MANNAN, S.L. and RODRIGUEZ, P., *J. Nucl. Mater.*, **102**, 7 (1981).
3. SEETHARAMAN, V., BHANU SANKARA RAO, K., MANNAN, S.L. and RODRIGUEZ, P., *Met. Sci. Eng.*, 63 (1984).
4. BHANU SANKARA RAO, K., SEETHARAMAN, V., MANNAN, S.L. and RODRIGUEZ, P., *Mater. Sci. Eng.*, 58 (1983).
5. BRINDLEY, B.J. and WORTHINGTON, P.J., *Met. Mater.*, **4**, 101 (1970).
6. CHICKERING, R.W., BAJAJ, R. and LALLY, J.S., in Proc. Radiation Effects in Breeder Reactor Structural Materials, eds. M.L. Bleiberg and J.W. Bennett, June 19–23, 1977, Scottsdale, Arizona, TMS–AIME, New York (1977).
7. MANNAN, S.L., SAMUEL, K.G. and RODRIGUEZ, P., *Trans. Ind. Inst. Metals*, **36**, 313 (1983).
8. COPLEY, S.M. and KEAR, B.H., *TMS-AIME*, **239**, 977 (1967).
9. COPLEY, S.M. and KEAR, B.H., *ibid.*, **239**, 984 (1967).
10. STOLOFF, N.S. and DAVIES, R.G., *Prog. Mater. Science*, **13**, 3 (1966).
11. BEARDMORE, P., DAVIES, R.G. and JOHNSTON, T.L., *TMS-AIME*, **245**, 1537 (1969).
12. STOLOFF, N.S., *Int. Met. Rev.*, **29**, 123 (1984).
13. POPE, D.P. and EZZ, S.S., *ibid*, **29**, 136 (1984).
14. BARNBY, J.T., *J. Iron Steel Inst.*, **203**, 392 (1965).
15. MICHEL, D.J., MOTEFF, J. and LOVELL, A.J., *Acta Met.*, **21**, 1269 (1973).
16. KUTUMBA RAO, V., TAPLIN, D.M.R. and RAMA RAO, P., *Met. Trans.*, **6A**, 77 (1975).
17. REED HILL, R.E., *Rev. High Temp. Mater.*, **2**, 214 (1974).
18. KOCH, C.C. and TROIANO, A.R., *Trans. ASM*, **57**, 519 (1964).
19. DE ALMEIDA, L.H. and MONTEIRO, S.N., Second International Conference on Mechanical Behaviour of Materials, 1697 (1976).
20. SHIOZAWA, K. and WEERTMAN, J.R., *Scripta Met.*, **15**, 1241 (1981).
21. KIKUCHI, M. and WEERTMAN, J.R., *Scripta Met.*, **14**, 797 (1980).
22. DYSON, B.F., LOVEDAY, M.S. and RODGERS, M.J., in Proc. Royal Society, London, A 349, 245 (1976).
23. NAZMY, M.Y. and DUERIG, T.W., *Scripta Met.*, **16**, 331 (1982).
24. MILLS, W.J., *Met. Trans.*, **11A**, 1039 (1980).
25. HALL, E.O., "Yield Point Phenomena in Metals and Alloys", Plenum Press (1970).

26. BAIRD, J.D., "The Inhomogeneity of Plastic Deformation", ASM, Metals Park, Ohio, p. 210 (1973).
27. RODRIGUEZ, P., *Bull. Mat. Sci.*, **6**, 653 (1984).
28. McCORMICK, P.G., *Acta Met.*, **20**, 351 (1972).
29. McCORMICK, P.G., Deformation – All Aspects, Intl. Conf. on Metal Science, ICMS, Ranchi (1983).
30. MULFORD, R.A., *Met. Trans.*, **10A**, 1527 (1979).
31. HAYES, R.W. and HAYES, W.C., *Acta Met.*, **30**, 1295 (1982).
32. JENKINS, C.F. and SMITH, G.V., *Trans. AIME*, **245**, 2149 (1969).
33. TAMHANKAR, R., PLATEAU, J. and CRUSSARD, C., *Rev. Met.*, **55**, 383 (1958).
34. SWALIN, R A. and MARTIN, A., *TMS-AIME*, **206**, 567 (1956).
35. KOUL, A.K. and PICKERING, F.B., *Scripta Met.*, **16**, 119 (1982).
36. DOI, H. and SHIMANUKI, Y., in Proc. 2nd International Conference on Superalloys – Processing, Champion, Pennsylvania (1972) (Metals and Ceramics Information Centre, Columbus, 1972, p 0–1).